Final Draft
of the original manuscript:

Davis, T.A.; Bichler, L.; D`Elia, F.; Hort, N.:
Effect of TiBor on the grain refinement and hot tearing susceptibility of AZ91D magnesium alloy.
In: Journal of Alloys and Compounds. Vol. 759 (2018) 70 - 79.
First published online by Elsevier: May 14, 2018

DOI: /10.1016/j.jallcom.2018.05.129
https://dx.doi.org/10.1016/j.jallcom.2018.05.129

Effect of TiBor on the grain refinement and hot tearing susceptibility of AZ91D magnesium alloy

T. A. Davis[1] and L. Bichler[1], F. D'Elia[2], N. Hort[2]

[1]University of British ColumbiaeOkanagan, School of Engineering, 3333 University Way, Kelowna, V1V 1V7, Canada
[2]Magnesium Innovation Centre, Helmholtz-Zentrum Geesthacht, D 21502 Geesthacht, Germany

Abstract

Hot tearing during solidification is frequently observed while casting alloys with a long freezing range (such as the AZ91D magnesium alloy) into molds with complex geometries and varying section thicknesses. Typically, hot tearing may be reduced or eliminated by manipulating the cooling rate, alloy composition or the mold geometry. These parameters directly influence the grain structure and interdendritic regions during the critical stage of an alloy's solidification when hot tears are prone to nucleate. In this work, the effect of a novel TiBor grain refiner on the hot tearing behavior of the AZ91D magnesium alloy was quantitatively studied. The relationship between the grain refinement level, the alloy's cooling rate and the in situ force evolution during casting solidification was investigated. The results revealed that for the AZ91D alloy, the force evolution rate and the microstructure were the critical determinants of the hot tearing severity. With the addition of the TiBor grain refiner, the grain size of the AZ91D alloy reduced by $\sim$70%, and the force and force-rate evolution significantly reduced as well, suggesting a homogenization of the internal stresses experienced by the solidifying alloy's microstructure, leading to a nearly complete elimination of hot tearing.

1 Introduction

Many automotive designers select magnesium (Mg) alloys for diverse structural applications. The Aluminum-Zinc (AZ) series magnesium alloys, such as the AZ91D alloy with 9 wt%Al, 1 wt%Zn and balance Mg, has been often used for thin-wall castings and parts with complex geometries [1]. The AZ-series casting alloys, however, have a long freezing range ($\sim$170 °C) and show a high propensity for hot tearing. Literature on the proposed mechanisms during hot tearing of Mg alloys has been published over the decades [2-5]. Despite the availability of literature, quantitative data on in situ alloy behavior is not readily available for shape castings of industrial relevance.

In general, hot tears nucleate at high solid fractions, fs, ($>\sim$0.8) and their growth is driven by the volumetric shrinkage of the alloy. If the metal's solidification shrinkage is constrained by a rigid casting mold, further enlargement of hot tears during thermal contraction of the casting ensues, often leading to a casting fracture [6-8]. Recent research [9,10] suggests that as solidification progresses after dendrite coherency, inadequate interdendritic feeding is unable to accommodate the solidification shrinkage of the alloy. The resulting micro-voids readily coalesce to form microscopic hot tears [11,12].

The severity of hot tearing is influenced by several factors: i) the alloy's cooling rate, ii) local stress and strain imposed on the microstructure, iii) rate of local stress and strain evolution, and iv) mold geometry [2,5,11]. A lower cooling rate may enable extended liquid metal flow through interdendritic channels, thus backfilling micro voids near the end of solidification [3,13,14]. However, slow cooling rates also result in undesirable and often excessive grain growth, resulting in a poor room temperature mechanical performance of the as-cast material.

Attempts to eliminate hot tearing via the microstructure engineering approach were reported in the literature. A key challenge associated with the dispersion of inoculants or modifiers in magnesium alloys is their flotation or settling, which is driven by the low density of the Mg matrix. In the case of the AZ91D alloy, modification of second phases [10,15] or grain refinement [16-18] were attempted. Modification often involved expensive rare earth (RE) elements added at high concentration levels, which created diverse phases at the grain boundaries, as well as in solid solution. However, grain refinement of aluminum-bearing Mg alloys remains difficult due to the Aluminum's ability to form intermetallic compounds with elements present in the additives and grain refiners. Therefore, a cost-effective modifier and a grain refiner for the most widely used industrial Mg alloys remains elusive [15].

In this research, casting experiments were conducted with a novel Al-Ti-B grain refiner prepared via an advanced powder metallurgy technique called spark plasma sintering (SPS). Published literature on the effectiveness of Al-Ti-B grain

refiners (also referred to as "TiBor" or "TiB grain refiner") in Mg alloys varies significantly [16-18] and most studies only report on the alloy's microstructure, with a limited discussion of casting defects. As a result, the present work provides an in-depth microstructural characterization of Al-Ti-B treated AZ91D magnesium alloy castings. Further, results of casting experiments with a mold instrumented with a load cell and thermocouples to quantify the effect of the TiBor grain refiner on the solidification and hot tearing of the AZ91D magnesium alloy are reported.

2 Experimental Procedure

2.1 Instrumentation

The steel mold used for all hot tearing experiments and in situ quantitative analysis of solidification and force evolution consisted of a vertical downsprue and a single horizontal bar oriented at 90° to the downsprue. A detailed description of the mold and associated instrumentation is available in the literature [4,11,13]. The load evolving in the horizontal bar during solidification and ensuing contraction was transferred from the horizontal bar via a threaded rod to an S-type load cell (Omega, LC101-500) and a data acquisition unit (Omega, OMB-DAQ-56). The DAQ operated at 2 scans/sec. A 0.5 mm (diam.) thermocouple (Omega, TJC36-CASS-020E-24) recorded solidification in a region adjacent to the 90° corner (where hot tears were seen to repeatedly form).

The mold temperature was controlled via electric resistance heaters (Omega, SWH171-020) connected to a PID controller (Omega, CN4316-DC1-R2). Casting trials with varying mold temperatures were carried out in triplicates to validate the repeatability of the observed hot tearing severity. As reported in the literature earlier [4,11,13] and validated in the present work, the level of hot tearing and trends recorded in situ exhibited excellent repeatability.

2.2 Grain refiner manufacture

A grain refiner was fabricated using the spark plasma sintering (SPS) powder metallurgical process. A Thermal Technology 10-3 SPS machine located at University of British Columbia's Okanagan campus, Kelowna, Canada, was used for grain refinement fabrication. The grain refiner was prepared by blending Titanium Aluminide (TiAl3) and Titanium Boride (TiB2) micro-scale powders with a 99.9% pure Al powder. Grain refiners with two concentrations were sintered: 1) Al-5Ti-1B (referred to as "Low TiBor"), and 2) Al-15Ti-3B (referred to as "High TiBor"). The powder blends were homogenized in a planetary ball mill and sub-

sequently sintered. For all casting experiments, 0.1 wt% of refiner was added to the AZ91D magnesium alloy.

2.3 Pouring process and casting parameters

Approximately 1 kg of AZ91D magnesium alloy was melted under a CO_2 atmosphere. Once the melt reached 740 °C, the TiBor grain refiner was introduced to the liquid alloy and stirred-in for 10 s. Then, the melt was allowed to stabilize for 2 min. Subsequently, the melt temperature was decreased to the pouring temperature of 720 °C, and a casting was made.

With the pouring temperature constant for all casting trials, three alloy compositions were prepared and studied: 1) pure (un-refined) AZ91D alloy, 2) AZ91D + Low TiBor alloy, and 3) AZ91D + High TiBor alloy. Based on preliminary trials (not reported here) by the authors on the effect of the mold temperature on the hot tearing susceptibility of the AZ91D alloy, at the 720 °C pouring temperature hot tears were eliminated at mold temperatures higher than 350 °C. Thus, the research results presented in this paper report on experiments at mold temperatures between 300 °C and 325 °C, which were observed to correspond to the onset temperatures for hot tearing.

2.4 Data analysis

The average cooling rate was calculated using the thermocouple placed in the casting mold. The time required to cool from the liquidus (TL) to the solidus (Ts) temperature was used to determine the average cooling rate. Also, the corresponding average force rate was calculated for this period using the magnitude of the load recorded at Ts.

Microstructure samples were extracted from the casting near the hot tearing region and ground with SiC papers (120 grit up to 600 grit) followed by diamond polishing (9 mme1 mm). Final polishing to a 0.05 mm surface finish was performed with colloidal alumina suspended in MeOH. Etching was completed using acetic glycol. A Zeiss Axiovert A1m optical microscope with Buehler OmniMet image analysis software was used for grain size analysis using the ASTM E112-13 standard [19]. The grain size values reported in this work were measured at the interior of the casting (i.e., away from the metal-mold interface). A Bruker Advance diffractometer with copper Cu K-α target was used for X-Ray Diffraction (XRD) analysis (scan angle from 0° to 110°, step size of 0.03° with a 90 s scan per interval). ICSD Database (FIZ-2009) was used for phase identification.

Electron Back Scatter Diffraction (EBSD) analysis was completed on a TESCAN Mira3 field emission scanning electron microscope (SEM) fitted with a Nordlys HKL EBSD detector. Each sample was scanned at a tilt angle of 70°

to the detector. A step size of 5.00 μm at 140° magnification was used for crystallographic texture and grain morphology analyses. Sample preparation for EBSD was the same as described above for optical analysis.

3 Results and discussion

3.1 Grain refiner

Fig.1 shows the microstructure of the as-sintered Low-TiBor and High-TiBor grain refiners fabricated via SPS. The increased inoculant concentration is clearly visible while comparing Fig. 1a and b. Both inoculating particles (i.e., large white $TiAl_3$ particles ($\sim$40 mm) and fine TiB_2 particles ($\sim$10 mm)) were homogeneously dispersed throughout the grain refiner's microstructure. During sintering, the primary objective was to consolidate a homogeneous blend of the powders, rather than fabricating high density grain refiners. As a result, as seen in Fig. 1c and d, voids near the large particles were often present. However, since the grain refiners dissolved upon addition to the liquid AZ91D magnesium alloy, the presence of porosity in the grain refiners was in fact beneficial to facilitate rapid grain refiner melting and subsequent release of the inoculants.

As observed in Fig. 1, a homogeneous dispersion of the inoculating particles was achieved during spark plasma sintering, despite their relatively high concentration. Published literature often suggests that when a high concentration of inoculating particles was present in a traditionally fabricated grain refiner (e.g., via extrusion), particle agglomeration readily occurred and caused an ineffective microstructure modification [16,17]. In addition to a homogeneous dispersion, however, the SPS process facilitated pre-wetting and diffusion of Al (from the grain refiner matrix) towards the inoculating particle's interior, as confirmed by SEM-XEDS linescans [23]. Such pre-wetting likely facilitated effective nucleation of $\{0001\}$ basal Mg planes on the $\{111\}$ planes of the aluminum pre-wetted inoculating particles [23].

3.2 General microstructure

Fig. 2 shows the general microstructure of the as-cast unrefined and refined AZ91D magnesium alloy castings. As can be observed, the grain size significantly decreased when the SPS TiBor grain refiners were added. In the case of the refined alloys, the grain boundaries were extensively covered with the eutectic β-phase ($Mg_{17}Al_{12}$), as expected, while the Mg_2Si and Al-Mn precipitates were generally dispersed across the microstructure. At both levels of TiBor refinement, the β-phase was more homogeneously distributed throughout the microstructure

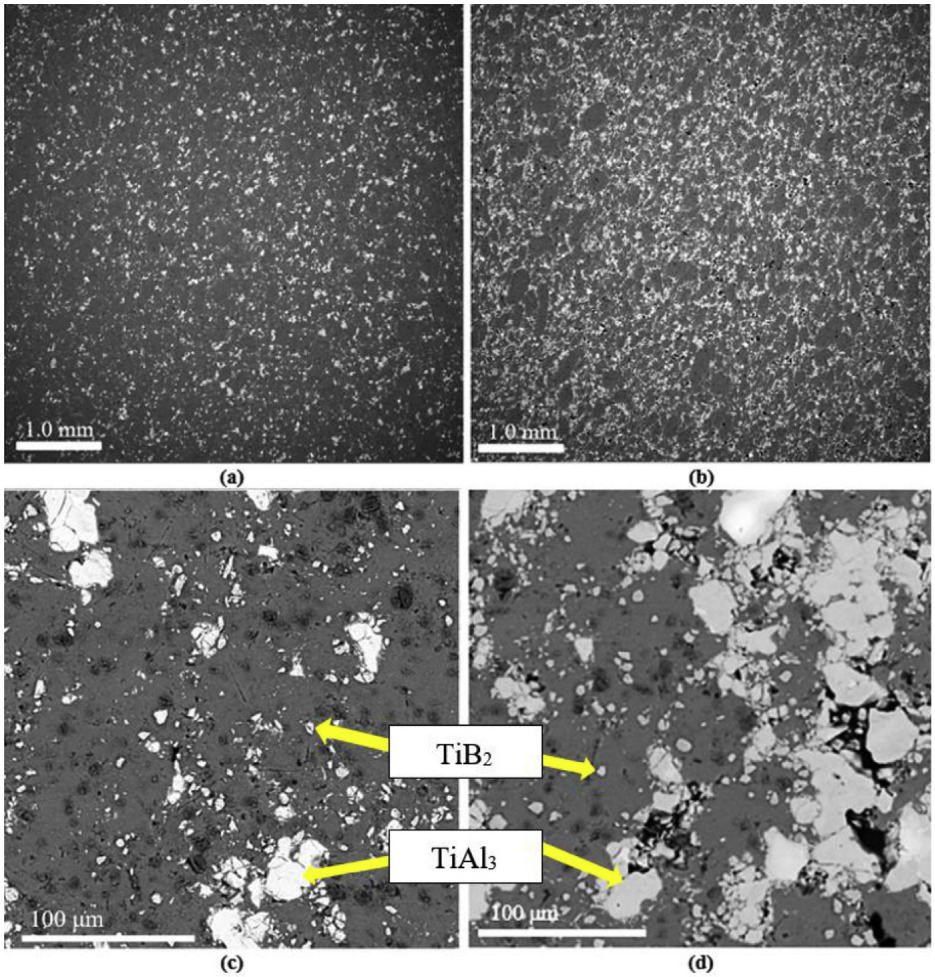

Figure 1: SEM micrographs of as-sintered SPS grain refiners: (a) Low TiBor (50x), (b) High TiBor (50x), (c) Low TiBor (1000x), (d) High TiBor (1000x).

than in the case of the unrefined AZ91D castings, indicating the possibility of a more uniform liquid feeding at high fractions of solid at the end of solidification. The Al-Mn and Mg_2Si precipitates in the unrefined castings were coarse and clearly visible, while in the refined castings these precipitates reduced in size and appeared more randomly dispersed.

Fig. 3 shows the results of grain size analysis (a minimum of 150 grains were measured for each condition). The grain size in the unrefined casting at 325 °C and 300 °C mold temperatures was ∼275 μm and ∼250 μm, respectively, with a relatively large standard deviation. Addition of the Low TiBor grain refiner reduced the grain size by ∼80% and ∼72% (grain size reached ∼60 μm and ∼73 μm) for the 325 °C and 300 °C mold temperatures, respectively. In the case of the High TiBor grain refiner, the grain size reduction was ∼72% and ∼70% (grain size reached ∼75 μm and ∼74 μm) for the two mold temperatures, respectively. Fig. 3 shows that the standard deviation significantly decreased with the addition of either of the grain refiners, suggesting a significant improvement in the grain size homogeneity across the casting.

Fig. 3 shows that the grain size of the unrefined castings increased with increasing mold temperature due to the alloy's known grain size dependency on the cooling-rate. For the TiBor refined castings, however, the grain size remained comparable (i.e., within the standard deviation) at both mold temperatures for both addition levels, suggesting that the grain refiner was highly effective, and its effect on grain size surpassed that of the cooling rate.

Measurement of the grain size variation across the casting's cross-section was also examined. As seen in Fig. 4, the grain size was measured at five locations across the horizontal bar's thickness (in the vicinity of the hot tear region). As can be seen in Fig. 5, the unrefined castings showed a large variation of grain size along the horizontal bar's cross section. The edges of the horizontal bar had finer grains (due to the mold interface and rapid cooling), while the grains at the center were significantly larger. In the case of the refined castings at both concentration levels and mold temperatures, the grain size at the outer edge and the center of the horizontal bar was comparable, indicating that the refiner induced heterogeneous nucleation throughout the entirety of the critical region and horizontal bar thickness.

3.3 Phase analysis

Fig. 6 shows the XRD plots of the unrefined and refined alloys, along with the spectrum for the grain refiners. Peaks representing the AZ91D magnesium alloy and its eutectic phase are also included. Fig. 6 shows that no new phases were detected in the refined alloys, possibly confirming that the TiBor additives were stable and did not react with the matrix during solidification to form new inter-

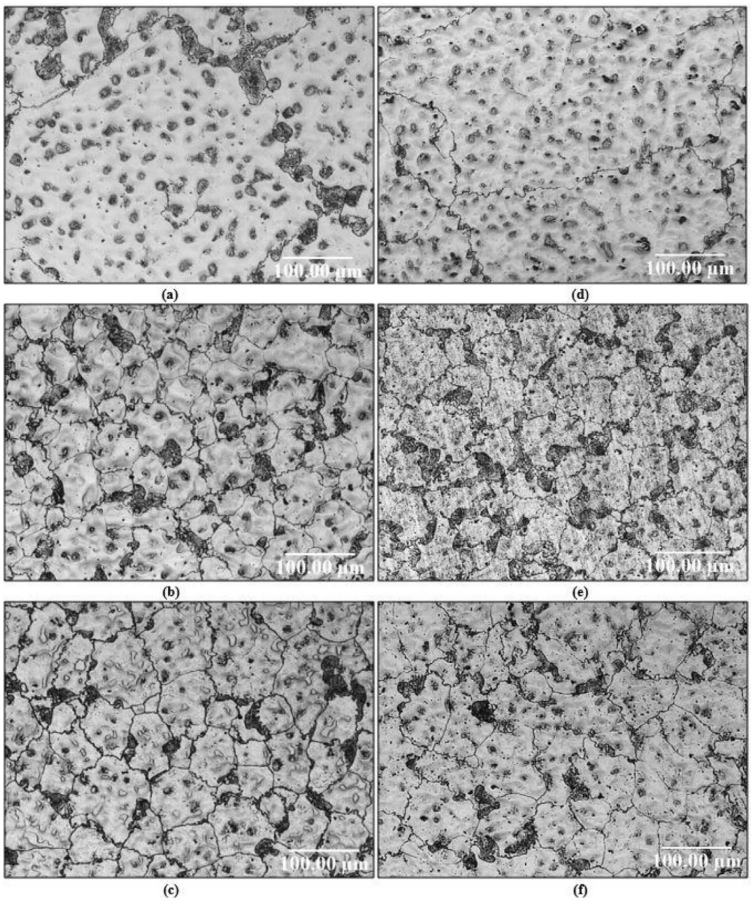

Figure 2: Effect of mold temperature (°C) and grain refinement (unrefined/Low TiBor/High TiBor) on the AZ91D alloy microstructure (200x magnification): (a) 325 °C Unrefined AZ91D, (b) 325 °C Low TiBor alloy, (c) 325 °C High TiBor alloy, (d) 300 °C Unrefined AZ91D alloy, (e) 300 °C Low TiBor alloy, (f) 300 °C High TiBor alloy.

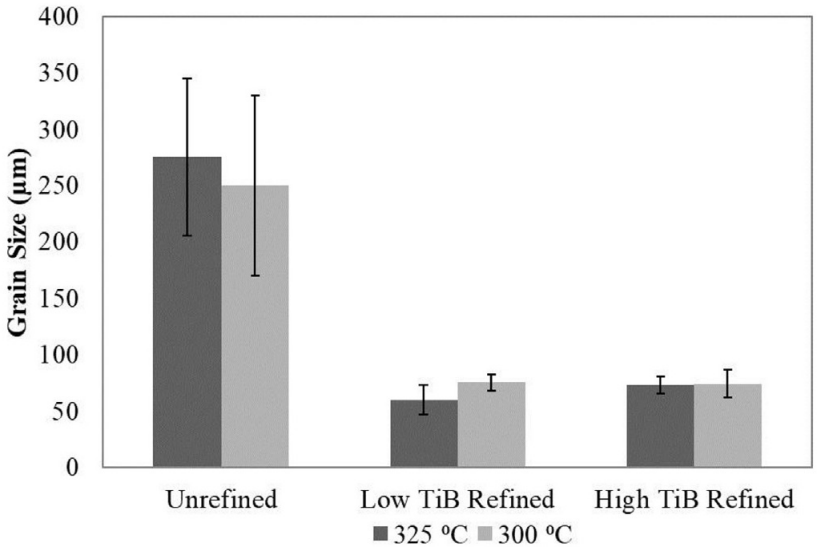

Figure 3: Effect of mold temperature and grain refiner concentration on the grain size.

metallics. However, it is recognized that the refiner particles were likely difficult to detect via XRD due to the minimum detectability limit of the XRD instrument.

A qualitative difference in the XRD plots for the unrefined and refined castings was observed for the α-Mg matrix $\{0001\}$ basal peak. Since, the XRD scans were performed in an area adjacent to the region with hot tears, the larger intensity of the basal peaks in the refined castings may indicate a higher volume fraction of grains oriented in a specific direction in the critical region where hot tears were generally observed. In the case of refined castings, the peak intensity remained comparable.

3.4 EBSD mapping and texture analysis

Directionally solidified castings often exhibit undesirable crystallographic texture. In the present work, the heat transfer in the horizontal bar was predominantly in the axial direction (i.e., directional solidification from the end of the horizontal bar towards the downsprue). EBSD mapping was carried out near the hot tear region with maps generated along a line from the center of the horizontal bar towards the mold interface. Fig. 7 shows the EBSD grain maps with grain size distribution, orientation and morphology.

The EBSD grain maps support the results of optical microscopy (Fig. 2). It was evident that a significant grain size reduction with the addition of a Low TiBor

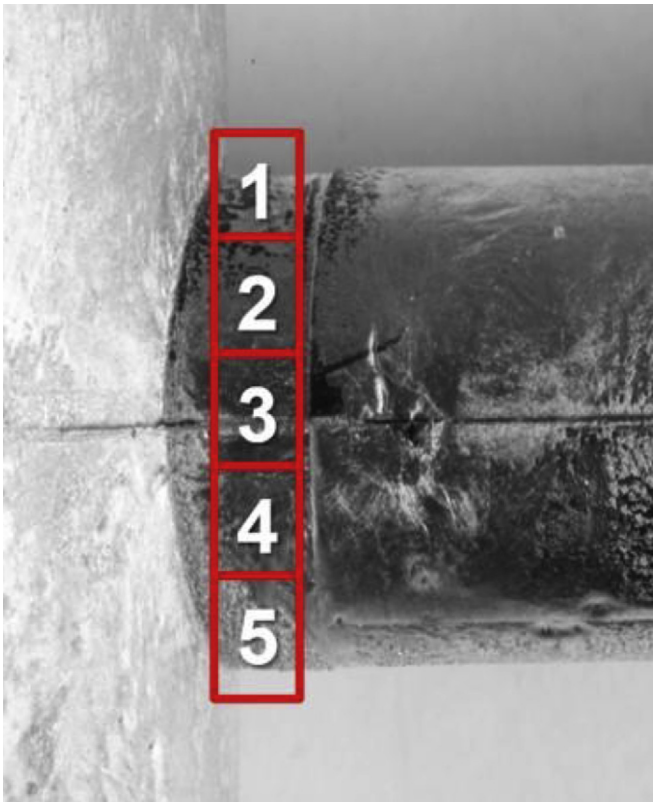

Figure 4: Regions of casting cross section with grain measurement locations.

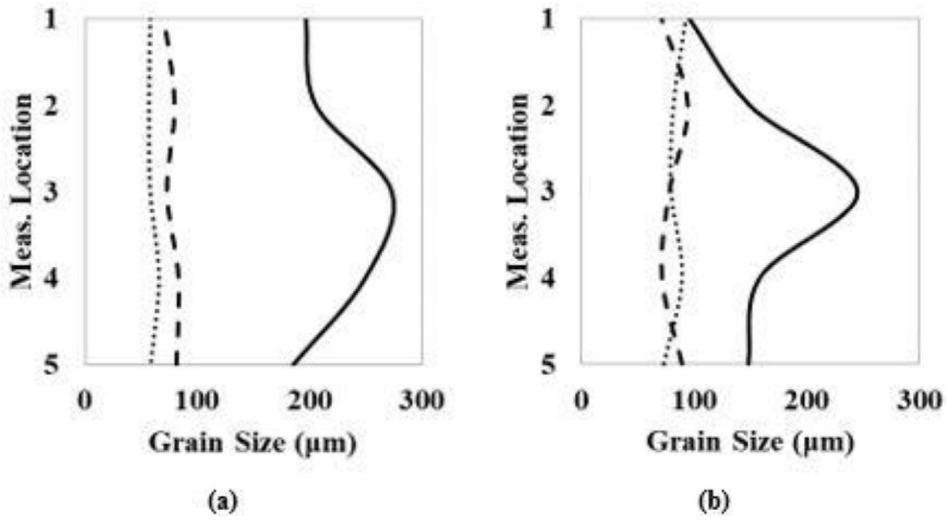

Figure 5: Grain size variation at the critical hot tear region for Unrefined (solid line), Low TiBor (dotted line), High TiBor (dashed line): (a) 325 °C mold temperature, (b) 300 °C mold temperature.

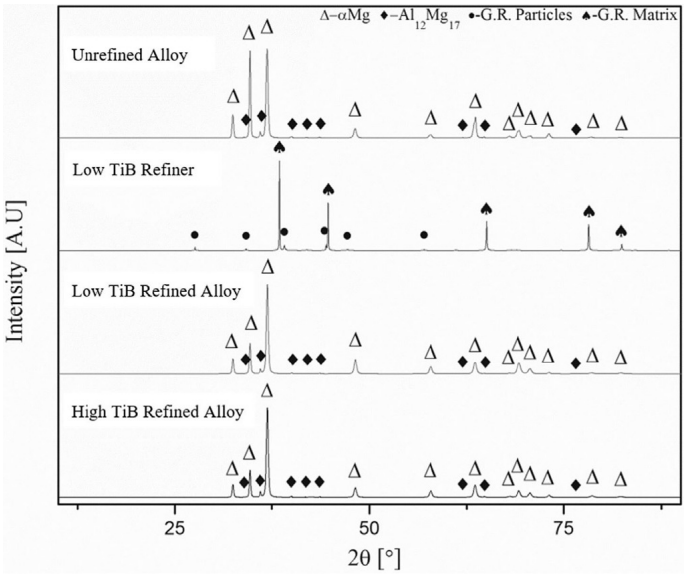

Figure 6: X-Ray diffractograms for alloy castings produced at 325 °C mold temperature.

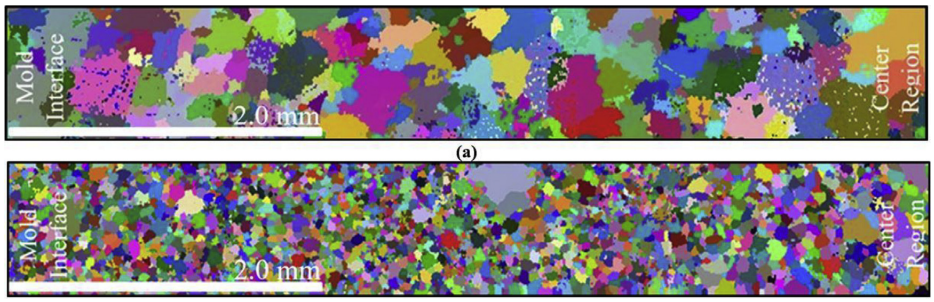

Figure 7: Representative EBSD grain maps of castings made at 325 °C mold temperature (140x magnification): (a) Unrefined AZ91D alloy, (b) AZ91D + Low TiBor alloy.

refiner was achieved. Except for a few large grains, the refined casting had a more uniform grain morphology across the entire scan area (i.e., from the horizontal bar towards the metal-mold interface) than the unrefined alloy.

Fig. 8 shows representative pole figures for the unrefined and the Low TiBor casting made at 325 °C mold temperature. The family of the {0001} basal planes were seen in previous studies to readily align in the direction of heat flow [20,21]. In the case of the unrefined casting in the present work, the {0001} planes exhibited nearly 3 times higher orientation densities (Maximum Uniform Density (MUD) of 7.70 for unrefined vs. 3.13 for refined casting), indicating a relatively stronger crystallographic texture in the direction of heat flow. Thus, the results suggest that the TiBor grain refiner was effective in reducing crystallographic texture in the critical region of the casting where hot tears typically nucleated.

3.5 Hot tear severity

Fig. 9 shows representative macrographs of hot tears near the junction between the downsprue and the horizontal bar. At relatively low mold temperatures (e.g., <300 °C), severe and continuous hot tears formed and fully encircled the horizontal bar. At 325 °C mold temperature, only a discontinuous hairline hot tear was observed, while at 350 °C mold temperatures and higher, no hot tears were visible on the casting surface. Thus, as expected with an increasing mold temperature, the hot tear severity decreased.

The hot tear nucleated at the stress concentration region (i.e., a 90° corner between the horizontal bar and the downsprue) and propagated via interdendritic regions in the direction of a decreasing stress gradient, as seen in Fig. 10. All castings with a hot tear exhibited this hot tear propagation direction.

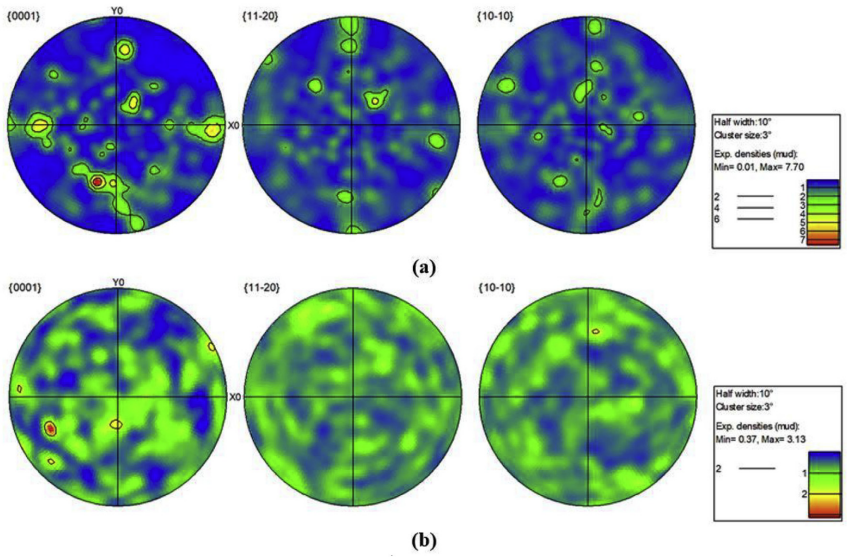

Figure 8: EBSD pole figures of castings produced at 325 °C mold temperature: (a) Unrefined AZ91D alloy, (b) AZ91D þ Low TiBor alloy.

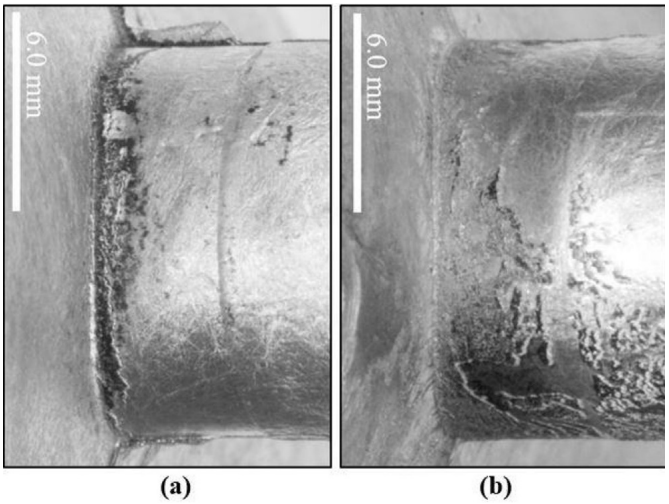

Figure 9: Macroscopic hot tear at the 90° junction: (a) 325 °C, and (b) 350 °C mold temperatures.

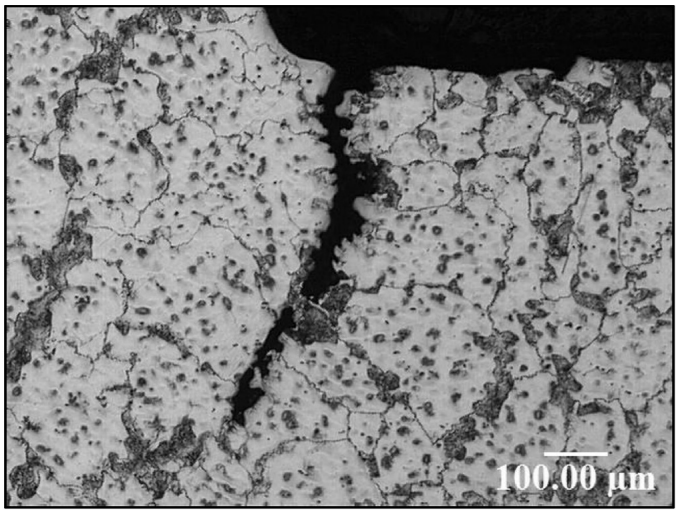

Figure 10: A representative intergranular hot tear in the unrefined casting at 325 °C mold temperature.

Fig. 11 shows representative hot tears for casting produced at the 325 °C mold temperature. In the case of the unrefined casting, the micro hot tear spanned several dendritic grains and reached ∼0.6 mm into the casting interior. In the Low TiBor grain refined casting, the micro hot tear only formed on the surface (i.e., a surface defect). In the High TiBor grain refined casting, the size of the hot tear further reduced and only surface interdendritic void was observed.

Fig. 12 shows that at 300 °C mold temperature, the severity of hot tears increased. In the unrefined casting, the hot tear reached a length of ∼1.8 mm from the casting surface towards the casting interior. The mating surfaces on either side of the hot tear, as well as the non-straight crack propagation path suggest a brittle-like fracture. For the Low TiBor grain refined alloy, an ∼0.4 mm long hot tear was visible near the casting exterior (i.e., skin region) and did not appear to extensively propagate towards the casting interior. This crack arrested within a few grains. Fig. 12c shows that a further increase of the grain refiner concentration only slightly reduced the hot tear length at this mold temperature.

A detailed examination of the hot tear fracture surface revealed that in both TiBor refined castings a continuous eutectic phase between grains may have healed micro porosity voids or even incipient hot tears. In contrast, the rough fracture surface observed in the unrefined AZ91D alloy castings suggests a typical brittle transgranular fracture due to inability of the microstructure to sustain evolving solidification stresses near the end of solidification [9,22]. Hence, the present results suggest that the refined alloys retained mobile eutectic liquid for a longer period during solidification, despite the higher cooling rates recorded during solidifica-

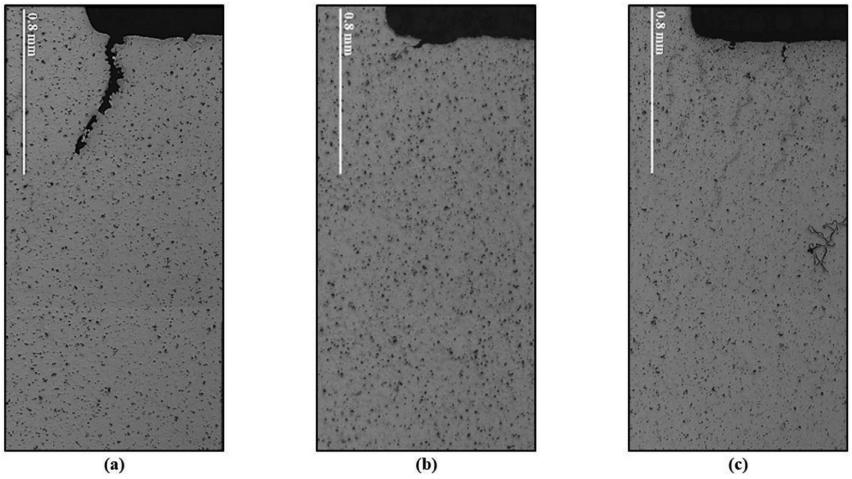

Figure 11: Macro view of stress concentration region and hot tears for castings made at 325 °C mold temperature: (a) Unrefined AZ91D alloy, (b) Low TiBor alloy, (c) High TiBor alloy.

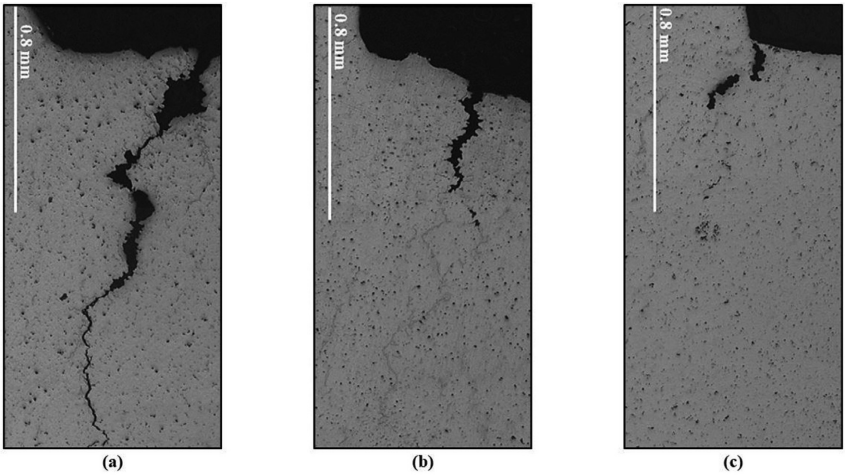

Figure 12: Macro view of stress concentration region and hot tears for castings made at 300 °C mold temperature: (a) Unrefined AZ91D alloy, (b) Low TiBor alloy, (c) High TiBor alloy.

tion. Enhanced interdendritic liquid feeding also reduced formation of shrinkage porosity, which is frequently considered the initial stage of hot tear development. These observations are further supported by the in situ force evolution measurements during casting solidification.

The exact role of the $TiAl_3$ particles on the hot tearing susceptibility of Mg alloys remains unresolved. Literature suggests that this phase may serve as a heterogeneous nucleation site and thus contribute to grain refinement in Mg alloys, yet it may negatively impact hot tearing due to its presence in the interdendritic regions and its obstruction of eutectic liquid flow at the end of solidification. Further, in the case of agglomerated $TiAl_3$ particles, they may also act as a stress concentration region in the microstructure, thus promoting the nucleation of hot tears [16]. In contrast, the $TiAl_3$ particles were also suggested to possibly dissolve above 700 °C, thereby releasing Ti and Al into the solution. Ti is known to restrict grain growth of the primary Mg phase, while Al would increase the volume fraction of the $Mg_{17}Al_{12}$ eutectic phase [17,18]. Both of these factors ought to decrease the alloy's hot tearing susceptibility. In the present work, hot tears propagated via interdendritic regions, which were generally free of the $TiAl_3$ phase, and therefore no deleterious effect of $TiAl_3$ was directly observed.

3.6 In situ force and cooling curves

The cooling curves in Fig. 13 reveal that for all castings solidification progressed similarly, and no exothermic peaks or solidification arrests observed for the refined castings. The cooling rates at 325 °C and 300 °C mold temperatures for the unrefined AZ91D castings were ∼1.6 °C/s and ∼3.1 °C/s, respectively. In the case of the Low TiBor alloy castings, the cooling rates were ∼2.3 °C/s and ∼4.1 °C/s, respectively, for the two mold temperatures. Finally, for the High TiBor alloy castings, the cooling rates were ∼2.1 °C/s and ∼3.6 °C/s, respectively. The increase in the cooling rate with the addition of the grain refiner may be a contributing factor to the reduction in the alloy's grain size, but was not likely the dominant factor. A reduction of cooling rate during solidification of grain refined alloys has been linked to grain growth restriction during solidification [16]. This contrasts with the present study, where an increase in cooling rate was observed as a result of grain refiner addition, which is often associated with an effective rapid heterogeneous inoculation of the melt. For example, the cooling rates at the lower mold temperature were almost twice in magnitude when compared to the unrefined casting; however, the reduction in grain size was minimal, as seen in Fig. 3. The precise mechanism responsible for the result in the present study remains the subject of further work [23].

The force rates at 325 °C and 300 °C mold temperature for the unrefined castings were ∼0.7 N/s and ∼1.6 N/s, respectively. For the same mold temperatures,

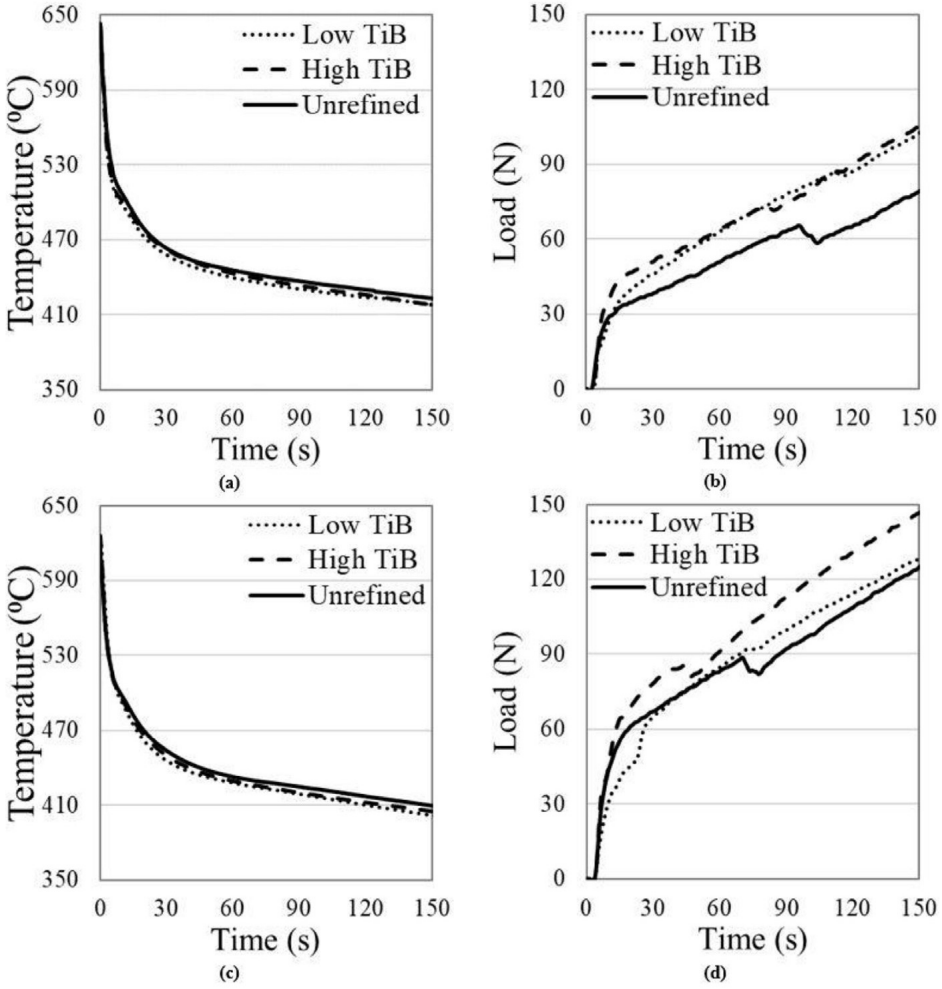

Figure 13: In situ cooling and force curves for castings with grain refinement produced at varying mold temperatures: (a) Cooling curves for 325 °C mold temperature castings, (b) Force curves for 325 °C mold temperature castings, (c) Cooling curves for 300 °C mold temperature castings, (d) Force curves for 300 °C mold temperature castings.

the Low TiBor casting experienced ∼0.9 N/s and 1.7 N/s, respectively. The High TiBor castings for the same temperatures had force rates of ∼1.0 N/s and ∼1.8 N/s, respectively. Although the force rates were comparable, the High TiBor casting experienced a slightly higher load at the end of solidification.

The solidification path of all castings followed a similar trend until the alloy reached ∼500 °C. At this temperature, the solidification paths began to diverge, where the refined castings consis-tently cooled at a higher rate. At the same temperature, the force curves began to exhibit a slope change, which was likely associated with the rigidity point of the AZ91D alloy [13], suggesting the force data captured the moment when the evolving dendritic microstructure was able to sustain solidification stresses.

Examining the difference in the force curves for the unrefined AZ91D and the TiBor refined castings, a small force release occurred at ∼10-20 s into the solidification process. This force release was reported to coincide with microporosity formation, grain boundary sliding, or a micro-hot tear nucleation [4,13]. For unrefined castings at both mold temperatures, this force relaxation occurred at ∼530 °C. A second large release in force was observed at ∼100 s for the 325 °C mold temperature casting and at ∼75 s for the 300 °C mold temperature casting. This force drop at the end of solidification was associated with the growth and propagation of a hot tear in the unrefined castings.

In the 325 °C mold temperature casting, at the Low TiBor and High TiBor addition levels, at ∼515 °C the first force drop was observed. However, due to the presence of the eutectic liquid along grain boundaries, as seen in Fig. 12b below the tear tip, the nucleating hot tears were possibly healed and did not further grow, despite the increasing solidification load. In the 300 °C mold temperature castings, a similar profile was also seen. Comparing the force curve results with the micrographs in Figs. 10 and 11, the tear severity observed was consistent with respect to the load events experienced in each casting at each mold temperature.

4 Conclusions

The results of the present study revealed that a TiBor grain refiner prepared by spark plasma sintering was capable of significantly refining the microstructure of an AZ91D permanent-mold cast alloy. The following conclusions stem from this work:

1. Microstructural refinement of AZ91D Mg alloy was successfully carried out, despite the presence of aluminum in the AZ91D alloy system. At both Low TiBor and High TiBor addition levels, a significant grain size reduction and a homogeneous dispersion of $Mg_{17}Al_{12}$ eutectic phase were achieved.

2. At both TiBor grain refiner concentration levels, a homogeneous grain size was observed throughout the casting's cross section, without the formation of new phases or crystallographic texture.

3. The TiBor grain refinement resulted in a significant decrease in the AZ91D alloy's susceptibility to hot tearing. Quantitative in situ force measurements revealed that a stress release (i.e., hot tear formation) did not occur at the end of solidification, likely due to a well permeable interdendritic eutectic network, and finely interlocked dendritic α-Mg structure.

Acknowledgements

The authors would like to acknowledge the financial support of NSERC Discovery grant.

References

1. M. Avedesian, H. Baker, ASM Specialty Handbook: Magnesium and Magnesium Alloys, ASM International, Materials Park, OH, USA, 1999.

2. L. Bichler, C. Ravindran, D. Sediako, Onset of hot tearing in AE42 magnesium alloy, Can. Metall. Q. 48 (2009) 81e89.

3. H. Huang, P.H. Fu, Y.X. Wang, L.M. Peng, H.Y. Jiang, Effect of pouring and mold temperatures on hot tearing susceptibility of AZ91D and Mg-3Nd-0.2Zn-Zr Mg alloys, Trans. Nonferrous Met. Soc. China 24 (2014) 922e929.

4. Z.S. Zhen, N. Hort, Y.D. Huang, O. Utke, N. Petri, K.U. Kainer, Hot tearing behaviour of binary Mg-1Al alloy using a contraction force measuring method, Int. J. Cast Met. Res. 29 (2009) 331e334.

5. G. Cao, I. Haygood, S. Kou, Onset of hot tearing in ternary Mg-Al-Sr alloy castings, Metall. Mater. Trans. 41 (2010) 2139e2150.

6. Y. Wang, B. Sun, Q. Wang, Y. Zhu, W. Ding, An understanding of the hot tearing mechanism in AZ91 magnesium alloy, Mater. Lett. 53 (2002) 35e39.

7. A. Stangeland, A. Mo, D. Eskin, Thermal strain in the mushy zone for aluminum alloys, Metall. Mater. Trans. 37 (2006) 705e714.

8. M.A. Easton, M.A. Gibson, S. Zhu, T.B. Abbott, An a priori hot-tearing indicator applied to die-cast magnesium-rare earth alloys, Metall. Mater. Trans. 45 (2014) 3586e3595.

9. M. Rappaz, J.-M. Drezet, M. Gremaud, A new hot-tearing criterion, Metall. Mater. Trans. 30 (1999) 449e455.

10. P. Gunde, A. Schiffl, P.J. Uggowitzer, Influence of yttrium additions on the hot tearing susceptibility of magnesium-zinc alloys, Mater. Sci. Eng. 527 (2010) 7074e7079.

11. Z. Wang, Y. Huang, A. Srinivasan, Z. Liu, F. Beckmann, K.U. Kainer, N. Hort, Experimental and numerical analysis of hot tearing susceptibility for Mg-Y alloys, J. Mater. Sci. 49 (2014) 353e362.

12. C. Davidson, D. Viano, L. Lu, D. StJohn, Observation of crack initiation during hot tearing, Int. J. Cast Met. Res. 19 (2006) 59e65.

13. Y.D. Huang, Z. Wang, A. Srinivasan, K.U. Kainer, N. Hort, Metallurgical characterization of hot tearing curves recorded during solidification of magnesium alloys, Acta Phys. Pol. A 122 (2012) 497e500.

14. S. Mihanyar, A. Mo, M. M'Hamdi, K. Ellingsen, Modeling of decohesion and the initiation of hot tearing in coherent mushy zones of metallic alloys, Metall. Mater. Trans. 42 (2011) 1887e1895.

15. D.H. StJohn, M. Qian, M. a. Easton, P. Cao, Z. Hildebrand, Grain refinement of magnesium alloys, Metall. Mater. Trans. 36 (2005) 1669e1679.

16. A. Elsayed, C. Ravindran, B.S. Murty, Effect of Al-Ti-B based master alloys on grain refinement and hot tearing susceptibility of AZ91E magnesium alloy, Mater. Sci. Forum 690 (2011) 351e354.

17. T.J. Chen, R.Q. Wang, Y. Ma, Y. Hao, Grain refinement of AZ91D magnesium alloy by Al-Ti-B master alloy and its effect on mechanical properties, Mater. Des. 34 (2012) 637e648.

18. A. Koltygin, V. Bazhenov, U. Mahmadiyorov, Influence of Ale5Tie1B master alloy addition on the grain size of AZ91 alloy, J. Magnes. Alloy. 5 (2017) 313e319.

19. ASTM E112-13: Standard Test Methods for Determining Average Grain Size, ASTM International, West Conshohocken, PA, 2013.

20. R. Chen, S. Liang, D. Wu, E. Han, Consideration of castability and formability for new magnesium alloys, O. J. Metal. 2 (2012) 8e17.

21. A. Elsayed, D. Sediako, C. Ravindran, Solidification analysis of a magnesium-zinc alloy using in-Situ neutron diffraction, in: Sha. Cast.: 6th Int. Sym., 2016, pp. 167e174.

22. D.G. Eskin, L. Katgerman, A quest for a new hot tearing criterion, Metall. Mater. Trans. 38 (2007) 1511e1519.

23. T. Davis, Analysis of Novel Grain Refinement in AZ91D Magnesium alloy with Quantitative Investigations on Hot Tearing, Ph.D Thesis, University of British Columbia, Kelowna, BC, Canada, 2018.